Steel and Composite Structures, *Vol*. *26*, *No*. *3* (*2018*) *273-287*
DOI: https://doi.org/10.12989/scs.2018.26.3.273

Buckling and free vibration analysis of FG-CNTRC-micro sandwich plate

Farzad Kolahdouzan [1a], Ali Ghorbanpour Arani [*1,2] and Mohammad Abdollahian [1b]

[1] *Faculty of Mechanical Engineering*, *University of kashan*, *Kashan*, *Iran*
[2] *Institute of Nanoscience & Nanotechnology University of Kashan*, *Kashan*, *Iran*

(*Received May 16, 2017, Revised September 24, 2017, Accepted October 22, 2017*)

Abstract. Buckling and free vibration analysis of sandwich micro plate (SMP) integrated with piezoelectric layers embedded in orthotropic Pasternak are investigated in this paper. The refined Zigzag theory (RZT) is taken into consideration to model the SMP. Four different types of functionally graded (FG) distribution through the thickness of the SMP core layer which is reinforced with single-wall carbon nanotubes (SWCNTs) are considered. The modified couple stress theory (MCST) is employed to capture the effects of small scale effects. The sandwich structure is exposed to a two dimensional magnetic field and also, piezoelectric layers are subjected to external applied voltages. In order to obtain governing equation, energy method as well as Hamilton's principle is applied. Based on an analytical solution the critical buckling loads and natural frequency are obtained. The effects of volume fraction of carbon nanotubes (CNTs), different distributions of CNTs, foundation stiffness parameters, magnetic and electric fields, small scale parameter and the thickness of piezoelectric layers on the both critical buckling loads and natural frequency of the SMP are examined. The obtained results demonstrate that the effects of volume fraction of CNTs play an important role in analyzing buckling and free vibration behavior of the SMP. Furthermore, the effects of magnetic and electric fields are remarkable on the mechanical responses of the system and cannot be neglected.

Keywords: buckling; free vibration; sandwich structure; RZT; MCST; Refined Zigzag Theory

1. Introduction

Recently, based on the properties of CNTs such as high strength and stiffness, high elastic medium and aspect ratio using these materials have been attracted many investigators (Esawi and Farag 2007, Salvetat and Rubio 2002, Fiedler *et al*. 2006). Actually, the extraordinary effects of CNTs make them excellent choice to reinforce polymer composites. In fact, investigating thermal and mechanical properties of functionally graded carbon nanotube-reinforced composites (FG-CNTRCs) have been considered by many investigators. Alibeigloo (2013) analyzed static behavior of FG-CNTRC plates embedded in piezoelectric layers using theory of elasticity. Mechanical and thermal post-buckling analysis of FG rectangular plates with various supported boundaries resting on nonlinear elastic foundation was studied by Zhang and Zhou (2015). Shen (2009) discussed nonlinear bending of FG-CNTRCs plates in thermal environments. He used many-body reactive empirical bond order potential to describe the interaction between carbon atoms. Moreover, he concluded that the variation of temperature reduces the elastic moduli and degrades the strength of the nano composites. Yas and Samadi (2012) carried out free vibration and buckling analysis of CNTRCs Timoshenko beams on elastic medium.

They considered four different distributions of CNTs to calculate frequency and critical buckling loads. They approved that, various distributions of CNTs have remarkable results on frequency and critical buckling loads of the structures. Differential cubature for vibration analysis of embedded FG-CNT- reinforced piezoelectric cylindrical shells subjected to uniform and non-uniform temperature distributionbs is carried out by Madani *et al*. (2016). Rabani Bidgoli *et al*. (2015) analyzed Viscous fluid induced vibration and instability of FG-CNT-reinforced cylindrical shells integrated with piezoelectric layers.

Classical sandwich structures consist of two faces which are made up high strength materials and one thicker layer called core. Recently, sandwich structures are vastly investigated due to their stupendous features such as high stiffness-to-weight and strength-to-weight ratios. Ramamoorthy *et al*. (2016) carried out vibration analysis of a partially treated laminated composite magnetorheological (MR) fluid sandwich plate. In fact, the core layer of this sandwich structure is composed of rubber and MR fluid. They concluded that, the size of MR fluid segment have noticeable effects on the natural frequency. Post-buckling behavior of composite and sandwich skew plates was investigated by Upadhyay and Shulka (2013). They considered higher order shear deformation theory for mathematical modeling of sandwich plates. They used finite degree double Chebyshev series method for employing spatial discretization of governing equations. Ferreira *et al*. (2008) analyzed static deformations and vibration analysis of composite and sandwich plates using a layerwise theory and radial basis function discretization with optimal shape

*Corresponding author, Ph.D., Professor,
E-mail: aghorban@kashanu.ac.ir
[a] Ms.C. Student, E-mail: F.kollahdouzan@gmail.com
[b] Ph.D. Student,
E-mail: abdollahianmohammad@yahoo.com

ISSN: 1229-9367 (Print), 1598-6233 (Online)

parameter. To increase the accuracy, the analysis was based on a new numerical scheme which was called radial basis functions. Moita *et al*. (2015) carried out buckling and geometrically nonlinear analysis of sandwich structures. They utilized Reddy's third order shear deformation theory for the core. In this paper continuity between the layers was satisfied. Recently, RZT, proposed by Tessler *et al*. (2009), has been utilized to simulate sandwich structures. This theory calculates highly accurate response prediction without using shear correction factor. In another study, Tessler *et al*. (2010) presented a consistent refinement of first order shear deformation theory for laminated composite and sandwich plates using improved zigzag kinematic. Therefore, they formulated RZT and compared accuracy of this theory with different ones. It was proved that, RZT is more accurate among other theories for sandwich plates. Iurlaro *et al*. (2013) carried out assessment of RZT for bending, vibration and buckling of sandwich plate. Similarly, they compared obtained results with other theories and evaluated the accuracy and quality of this theory. Ghorbanpour Arani *et al*. (2016) analyzed RZT for vibration analysis of viscoelastic FG-CNTRC micro plates integrated with piezoelectric layers. In another paper, buckling and post-buckling analyses of piezoelectric hybrid microplate subject to thermo-electro-mechanical loads based on the MCST were investigaed by Lou *et al*. (2016). The Mindlin plate theory is adopted to describe its deflection behavior with the von Karman's geometric nonlinearity taken into account. It is ascertained, increment of material length scale parameter leads to increasing the dimensionless compressive load. Meanwhile, the effects of electric field on the dimensionless compressive load were shown. They concluded with increasing of electric field dimensionless load become less and vice versa. Also, Lou and He (2015) carried out closed-form solutions for nonlinear bending and free vibration of FG microplates based on the MCST. It is shown that increment of material length scale parameter leads to increasing the dimensionless frequency and decrement of deflection.

Since it is demonstrated that in micro- and nano-scale, classical elasticity theory is not capable of size effects. Therefore, it is necessary to employ higher order continuum theories such as nonlocal elasticity theory, modified couple stress and modified strain gradient theories. Size dependent buckling analysis of functionally graded micro beams based on MCST was presented by Nateghi *et al*. (2012). Their analysis was done with three different theories: classical, first and third order shears deformation beam theories. Li and Pan (2015) evaluated static bending and free vibration of a FG piezoelectric microplate based on MCST. They extended concept of functionally graded material (FGM) into the piezoelectric material which was called functionally graded piezoelectric materials (FGPMs). Mohammad-Abadi and Daneshmehr (2014) carried out size dependent buckling analysis of microbeams based on MCST with higher order theories and general boundary conditions. They used Euler-Bernoulli, Timoshenko and Reddy beam theories to simulate the microbeam and generalized differential quadrature (GDQ) as well as analytical methods to solve the governing equations. A MCST for buckling analysis of sigmoid-FGM nanoplates embedded in Pasternak elastic medium was discussed by Jung *et al*. (2014). Ghorbanpour Arani *et al*. (2015a) studied vibration of bioliquid-filled microtubules embedded in cytoplasm including surface effects using MCST.

Imposing magnetic field to CNTs can be an effective parameter to control the mechanical responses of them. Therefore, magnetic field can be applied as a controller parameter in structures reinforced with CNTs, too. According to this fact, many investigations have been done to study the influences of magnetic field on the mechanical responses of CNTs and also structures reinforced with CNTs. Wave propagation in single-walled carbon nanotube under longitudinal magnetic field using nonlocal Euler-Bernoulli beam theory was researched by Narendar *et al*. (2012). The governing equations of motion have been derived by considering Lorentz magnetic force obtained from Maxwell's relations. They found that nonlocality declines the wave velocity. Kiani (2014a) evaluated free vibration of conducting nanoplates exposed to unidirectional in-plane magnetic fields using nonlocal shear deformable plate theories. Characterization of free vibration of elastically supported double-walled carbon nanotubes subjected to a longitudinally varying magnetic field was presented by Kiani (2013). In this work frequencies as well as the corresponding vibration modes are evaluated for different varying magnetic fields. The obtained results display that the flexural frequencies magnify with the magnetic field strength. The effect of variation of the axial magnetic field on the vibrational mode patterns of both the innermost and outermost tubes is also illustrated. In another paper, Kiani (2014b) investigated magnetically affected SWCNTs as nanosensors. This is shown that the mechanical sensing of SWCNTs is enhanced by application of the longitudinal magnetic field. Revisiting the free transverse vibration of embedded single-layer graphene sheets acted upon by in-plane magnetic field was performed by Kiani (2014c). Elastic wave propagation in magnetically affected double-walled carbon nanotubes was carried out by Kiani (2015a). In another paper, Kiani (2015b) Column buckling of magnetically affected stocky nanowires carrying electric current. By adopting Gurtin–Murdoch surface elasticity theory, the governing equations of the nanostructure are obtained based on the Timoshenko and higher-order beam models. The results show that the surface energy effect becomes important in buckling behavior of the current carrying nanowires.

To the best of our knowledge, the mechanical responses of SMP have not been received enough attentions so far. Motivated by these considerations, the main purposes of this paper are to study the buckling and free vibration analysis of SMPs resting on elastic foundation. The core layer which is integrated with ZnO layers, is reinforced with four type of different distributions of CNTs along the thickness direction. The SMP is subjected to 2D magnetic field so that the CNTs respond as they are exposed to magnetic field. Accordingly, magnetic field and external applied voltages play an inevitable role in mechanical responses of SMP. Theoretical formulations of sandwich structure are presented based on RZT. The MSCT is

employed to consider size effects. To achieve the governing motion equations, energy method and Hamilton's principle is applied and using an analytical solution the critical buckling loads and natural frequency are obtained. The effects of small scale parameter, electric and magnetic loadings, distribution of CNTs, elastic foundation, thickness of each layer and mode numbers on the buckling and natural frequency of SMP are illustrated.

2. Mechanical formulations

Fig. 1 shows a schematic geometry of a sandwich pale integrated with two piezoelectric layers as actuators and embedded in orthotropic Pasternak foundation. As seen in Fig. 1, h_t, a, b describe the total thickness, length and width of the structure, respectively. h_1 is the thickness of lower and upper layers and h_m represents the and core layer thickness.

2.1 Material properties of CNTRC plates

As stated above, in this work different distributions of CNTs such as uniformly distributed (UD), $FG-\Lambda$, $FG-X$ and $FG-O$ are considered. With respect to the rule of mixture, the effective mechanical properties of the CNTRC microplate (effective Young's modulus and shear modulus) can be expressed as Alibeigloo (2013)

$$E_{11} = \eta_1 V_{cnt} E_{11}^{cnt} + V_m E^m, \tag{1a}$$

$$\frac{\eta_2}{E_{22}} = \frac{V_{cnt}}{E_{22}^{cnt}} + \frac{V_m}{G^m}, \tag{1b}$$

$$\frac{\eta_3}{G_{12}} = \frac{V_{cnt}}{G_{12}^{cnt}} + \frac{V_m}{G^m}, \tag{1c}$$

where E_{11}^{cnt}, E_{22}^{cnt} and G_{12}^{cnt} are the Young's moduli and shear modulus of SWCNT, respectively. G^m and E^m indicate the corresponding properties of the isotropic matrix, respectively. η_j (j = 1, 2, 3) is the CNT efficiency parameter. V_{cnt} and V_m are the CNT and matrix volume fractions and are related by

$$V_m + V_{cnt} = 1. \tag{2}$$

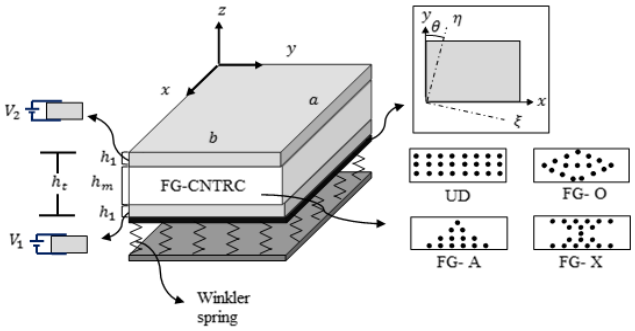

Fig. 1 Configuration of sandwich micro plate

The following equations can be written to express the relation of mass density ρ and Poisson's ratio υ as follows

$$\upsilon_{12} = V_{cnt} \upsilon_{12}^{cnt} + V_m \upsilon^m, \tag{3a}$$

$$\rho = V_{cnt} \rho^{cnt} + V_m \rho^m, \tag{3b}$$

Poisson's ratios of matrix and CNT, respectively. Also, different volume fractions for uniform distributions and other three FG distributions of the CNTs along the thickness z direction can be described as

$$UD: \quad V_{cnt} = V_{cnt}^*, \tag{4a}$$

$$FG-\Lambda: \quad V_{cnt} = \left(1 + 2\frac{z}{h}\right) V_{cnt}^*, \tag{4b}$$

$$FG-X: \quad V_{cnt} = 4\frac{|z|}{h} V_{cnt}^*, \tag{4c}$$

$$FG-O: \quad V_{cnt} = 2 - 4\frac{|z|}{h} V_{cnt}^*, \tag{4d}$$

where V_{cnt}^* can be described as:

$$V_{cnt}^* = \frac{W_{cnt}}{W_{cnt} + (\rho^{cnt} / \rho^m)(1 - W_{cnt})}, \tag{5}$$

in which W_{cnt} is the mass fraction of CNTs.

2.2 Modified couple stress theory

In nanotechnology problems, it is necessary to consider small length-scale. The benefits of MCST are using only one length scale parameter and assuming symmetry of couple stress tensor. It should be mentioned that, the strain energy density is associated with strain and symmetric part of the curvature tensor. The strain energy occupying region V can be written as Li and Pan (2015)

$$U = \frac{1}{2}\int_V \left(\sigma_{ij}^k \varepsilon_{ij}^k + m_{ij}^k \chi_{ij}^k\right) dV, \ (i, j = x, y, z), \tag{6}$$

where χ_{ij}^k is the symmetric curvature tensors, ε_{ij}^k is the strain tensor and the superscript k = (a, b and c) represent the lower layer, core layer and upper layer, respectively. Therefore, the components of rotation vector of k^{th} layer, θ_i^k, electric field, E_{ii}, symmetric curvature tensors and strain tensor can be written as follows

$$\varepsilon_{ij}^k = \frac{1}{2}\left(u_{i,j}^k + u_{j,i}^k\right), \tag{7a}$$

$$\chi_{ij}^k = \frac{1}{2}\left(\theta_{i,j}^k + \theta_{j,i}^k\right), \tag{7b}$$

$$\theta_i^k = \frac{1}{2}\left(curl\left(u_i^k\right)\right), \tag{7c}$$

$$E_{ii}^{k} = -\Phi_{\alpha,ii}\,,\ (\alpha=1,2), \tag{7d}$$

where u_i^k are components of displacement vector and Φ is electric potential distribution in the thickness direction. The constitutive relations for SMP can be described as

$$\sigma_{ij}^{k} = Q_{ijnl}^{k}\varepsilon_{nl}^{k} + e_{ijn}^{k}E_{n}^{k}\,, \tag{8a}$$

$$D_{ii}^{k} = e_{inl}^{k}\varepsilon_{nl}^{k} + \mu_{in}^{k}E_{n}^{k}\,, \tag{8b}$$

$$m_{ij}^{k} = 2Q_{44}^{k}l^{2}\chi_{ij}^{k}\,, \tag{8c}$$

where σ_{ij}^k, D_{ij}^k, m_{ij}^k, Q_{ijnl}^k, e_{ijn}^k and μ_{in}^k are stress, electric displacement, couple stress tensor, the elastic, piezoelectric and dielectric coefficients, respectively. Also, l is the material length scale parameter measuring the couple stress effect.

2.3 Refined zigzag theory

In this paper, in order to simulate the sandwich structure RZT have been applied Tessler *et al*. (2010); in which displacement components vector of the k[th] layer of the structure U_1^k, V_1^k and W_1 along the coordinate directions *x*, *y* and *z* respectively, are written as

$$\begin{aligned} U_1^{k}(x,y,z,t) = {} & u(x,y,t) + z\,\theta_1(x,y,t) \\ & + \phi_1^{k}(z)\ \psi_1(x,y,t), \end{aligned} \tag{9a}$$

$$\begin{aligned} V_1^{k}(x,y,z,t) = {} & v(x,y,t) + z\,\theta_2(x,y,t) \\ & + \phi_2^{k}(z)\ \psi_2(x,y,t), \end{aligned} \tag{9b}$$

$$W_1(x,y,z,t) = w(x,y,t), \tag{9c}$$

where *u*, *v* and *w* are the components of mid-plate and *t* represents the time. θ_1 and θ_2 are also, bending rotations of the transverse normal about the positive *y* axis and the negative *x* axis directions, respectively. ψ_1 and ψ_2 describe the spatial amplitudes of zigzag rotation. The advantage of RZT over other theories for sandwich structures, is adopting zigzag function $\phi_\alpha^k(z)$, (α = 1, 2) which is related to the thickness and elastic stiffness coefficients of each layer. Using Eqs. (7), the strain and curvature components can be expressed as

$$\varepsilon_{xx}^{k} = u_{,x} + z\,\theta_{1,x} + \phi_1^{k}\psi_{1,x}\,, \tag{10a}$$

$$\varepsilon_{yy}^{k} = v_{,y} + z\,\theta_{2,y} + \phi_2^{k}\psi_{2,y}\,, \tag{10b}$$

$$\begin{aligned} \gamma_{xy}^{k} = {} & v_{,x} + z\,\theta_{2,x} + \phi_2^{k}\psi_{2,x} + u_{,y} + z\,\theta_{1,y} \\ & + \phi_1^{k}\psi_{1,y}\,, \end{aligned} \tag{10c}$$

$$\gamma_{zx}^{k} = w_{,x} + \theta_1 + \phi_{1,z}^{k}\psi_1, \tag{10d}$$

$$\gamma_{zy}^{k} = w_{,y} + \theta_2 + \phi_{2,z}^{k}\psi_2, \tag{10e}$$

$$\chi_{xx}^{k} = 1/2w_{,xy} - 1/2\theta_{2,x} - 1/2\phi_{2,z}^{k}\psi_{2,x}\,, \tag{10f}$$

$$\chi_{yy}^{k} = -1/2w_{,xy} + 1/2\,\theta_{1,y} + 1/2\phi_{1,z}^{k}\psi_{1,y}\,, \tag{10g}$$

$$\begin{aligned} \chi_{zz}^{k} = {} & 1/2\theta_{2,x} + 1/2\phi_{2,z}^{k}\psi_{2,x} - 1/2\theta_{1,y} \\ & - 1/2\phi_{1,z}^{k}\psi_{1,y}\,, \end{aligned} \tag{10h}$$

$$\begin{aligned} \chi_{xy}^{k} = {} & 1/2w_{,yy} - 1/2\theta_{2,y} - 1/2\,\phi_{2,z}^{k}\psi_{2,y} \\ & - 1/2w_{,xx} + 1/2\theta_{1,x} + 1/2\phi_{1,z}^{k}\psi_{1,x}\,, \end{aligned} \tag{10i}$$

$$\begin{aligned} \chi_{zx}^{k} = {} & 1/2v_{,xx} + 1/2z\,\theta_{2,xx} + 1/2\phi_2^{k}\psi_{2,xx} \\ & - 1/2u_{,xy} - 1/2z\,\theta_{1,xy} - 1/2\phi_1^{k}\psi_{1,xy}\,, \end{aligned} \tag{10j}$$

$$\begin{aligned} \chi_{zy}^{k} = {} & 1/2v_{,xy} + 1/2z\,\theta_{2,xy} + 1/2\phi_2^{k}\psi_{2,xy} \\ & - 1/2u_{,yy} - 1/2z\,\theta_{1,yy} - 1/2\phi_1^{k}\psi_{1,yy}\,, \end{aligned} \tag{10k}$$

Since the core layer of SMP integrated with piezoelectric layers, the following relations can be written for upper and lower layers Ghorbanpour Arani *et al*. (2016)

$$\begin{aligned} \Phi_1(x,y,z,t) = {} & \sin\left(\pi\left(-z-\frac{h_m}{2}\right)\Big/h_1\right)\varphi_1(x,y,t) \\ & + \left(-z-\frac{h_m}{2}\right)V_1\Big/h_1\,, \end{aligned} \tag{11a}$$

$$\begin{aligned} \Phi_2(x,y,z,t) = {} & \sin\left(\pi\left(z-\frac{h_m}{2}\right)\Big/h_1\right)\varphi_2(x,y,t) \\ & + \left(z-\frac{h_m}{2}\right)V_2\Big/h_1\,, \end{aligned} \tag{11b}$$

where φ_1 and φ_2 describe spatial distribution of electric potentials, V_1 and V_2 indicate the external applied voltages on actuator layers. The constitutive equation for local stresses, electric displacements for the k^{th} layer of the SMP are

$$\begin{aligned} \begin{Bmatrix}\sigma_{xx}\\ \sigma_{yy}\\ \sigma_{yz}\\ \sigma_{zx}\\ \sigma_{xy}\end{Bmatrix}^{k} = {} & \begin{bmatrix} Q_{11} & Q_{12} & 0 & 0 & 0\\ Q_{21} & Q_{22} & 0 & 0 & 0\\ 0 & 0 & Q_{44} & 0 & 0\\ 0 & 0 & 0 & Q_{55} & 0\\ 0 & 0 & 0 & 0 & Q_{66}\end{bmatrix}^{k}\begin{Bmatrix}\varepsilon_{xx}\\ \varepsilon_{yy}\\ \gamma_{yz}\\ \gamma_{zx}\\ \gamma_{xy}\end{Bmatrix}^{k} \\ & - \begin{bmatrix} 0 & 0 & e_{31}\\ 0 & 0 & e_{32}\\ 0 & e_{24} & 0\\ e_{15} & 0 & 0\\ 0 & 0 & 0\end{bmatrix}^{k}\begin{Bmatrix}E_{xx}\\ E_{yy}\\ E_{zz}\end{Bmatrix}^{k}, \end{aligned} \tag{12a}$$

$$\begin{Bmatrix} D_{xx} \\ D_{yy} \\ D_{zz} \end{Bmatrix}^k = \begin{bmatrix} 0 & 0 & 0 & e_{15} & 0 \\ 0 & 0 & e_{24} & 0 & 0 \\ e_{31} & e_{32} & 0 & 0 & 0 \end{bmatrix}^k \begin{Bmatrix} \varepsilon_{xx} \\ \varepsilon_{yy} \\ \gamma_{yz} \\ \gamma_{zx} \\ \gamma_{xy} \end{Bmatrix}^k + \begin{bmatrix} \mu_{11} & 0 & 0 \\ 0 & \mu_{22} & 0 \\ 0 & 0 & \mu_{33} \end{bmatrix}^k \begin{Bmatrix} E_{xx} \\ E_{yy} \\ E_{zz} \end{Bmatrix}^k, \tag{12b}$$

where Shen (2009)

$$\begin{aligned} &Q_{11}^k = \frac{E_{11}^k}{1-\upsilon_{12}\upsilon_{21}},\ Q_{22}^k = \frac{E_{22}^k}{1-\upsilon_{12}\upsilon_{21}}, \\ &Q_{12}^k = \frac{\upsilon_{21}E_{11}^k}{1-\upsilon_{12}\upsilon_{21}} Q_{44}^k = \frac{E_{11}^k}{2\left(1+\upsilon_{12}\right)} = Q_{55}^k = Q_{66}^k, \end{aligned} \tag{13}$$

where E_{11}^k and E_{22}^k are effective Young's moduli of each layers; Q_{44}^k, Q_{55}^k and Q_{66}^k are the shear moduli and υ_{12} and υ_{21} describe the Poisson's ratios.

3. Equations of motion

The Hamilton's principle may be written as follows

$$\int_{t_0}^{t_1} \left[\delta U - \delta W - \delta K\right] dt = 0, \tag{14}$$

where δU, δW and δK are the variations of strain energy, external works and kinetic energy, respectively.

3.1 Strain energy

Eq. (6) is rewritten to obtain the strain energy of SMP as

$$\begin{aligned} U = &\frac{1}{2}\int_A \int_{-\frac{h_t}{2}}^{\frac{h_t}{2}} \left(\sigma_{xx}^k \varepsilon_{xx}^k + \sigma_{yy}^k \varepsilon_{yy}^k + \sigma_{xy}^k \gamma_{xy}^k + \sigma_{xz}^k \gamma_{xz}^k \right. \\ &\left. + \sigma_{yz}^k \gamma_{yz}^k - D_{xx}^k E_{xx}^k - D_{yy}^k E_{yy}^k - D_{zz}^k E_{zz}^k \right) dz dA \\ &+ \frac{1}{2}\int_A \int_{-\frac{h_t}{2}}^{\frac{h_t}{2}} \left(m_{xx}^k \chi_{xx}^k + m_{yy}^k \chi_{yy}^k + m_{zz}^k \chi_{zz}^k + m_{xy}^k \chi_{xy}^k \right. \\ &\left. + m_{xz}^k \chi_{xz}^k + m_{yz}^k \chi_{yz}^k \right) dz dA, \end{aligned} \tag{15}$$

Substituting Eqs. (10) to (12) into Eq. (15) yields

$$\begin{aligned} U = &\frac{1}{2}\int_A \left(N_{xx} u_{,x} + M_{xx} \theta_{1,x} + M_{xx}^{\phi 1} \psi_{1,x} + M_{xy} \theta_{2,x} \right. \\ &+ M_{xy}^{\phi 2} \psi_{2,x} + N_{xy}\left(u_{,y} + v_{,x}\right) + M_{xy} \theta_{1,y} \\ &+ M_{xy}^{\phi 1} \psi_1 + N_{yy} v_{,y} + M_{yy} \theta_{2,y} + M_{yy}^{\phi 2} \psi_2 \\ &+ Q^{\phi 1} \psi_1 + Q_2\left(w_{,y} + \theta_2\right) + Q^{\phi 2} \psi_2 + L_{xx} \varphi_{1,x} \\ &+ L_{yy} \varphi_{1,y} - L_{zz} \pi \varphi_1 / h_1 + Q_1\left(w_{,x} + \theta_1\right) \\ &\left. + L_{2xx} \varphi_{2,x} + L_{2zz} \pi \varphi_2 / h_1 + L_{2yy} \varphi_{2,y} \right) dA \\ &+ \frac{1}{2}\int_A \left(1/2 P_{xx}\left(\theta_{2,xy} - \theta_{2,x}\right) - 1/2 A_{xx}^{\phi 2} \psi_{2,x} \right. \\ &+ 1/2 A_{yy}^{\phi 1} \psi_{1,y} + 1/2 P_{yy}\left(-w_{,xy} + \theta_{1,y}\right) \\ &+ 1/2 P_{zz}\left(\theta_{2,x} - \theta_{1,y}\right) - 1/2 A_{zz}^{\phi 1} \psi_{1,y} + 1/2 A_{zz}^{\phi 1} \psi_{1,x} \\ &+ 1/2\left(w_{,yy} - \theta_{2,y} - w_{,yy} + \theta_{1,x}\right) P_{xy} + 1/2 A_{zz}^{\phi 2} \psi_{2,x} \\ &- 1/2 A_{zz}^{\phi 2} \psi_{2,y} + 1/2 S_{xz} \theta_{2,xx} + 1/2 S_{xz}^{\phi 2} \psi_{2,xx} \\ &+ 1/2 P_{xz}\left(v_{,xx} - u_{,xy}\right) + 1/2 P_{yz}\left(v_{,xy} - u_{,yy}\right) \\ &- 1/2 S_{xz} \theta_{1,xy} - 1/2 S_{xz}^{\phi 1} \psi_{1,xy} - 1/2 S_{yz}^{\phi 1} \psi_{1,yy} \\ &\left. - 1/2 S_{yz}\left(\theta_{1,yy} + \theta_{2,xy}\right) + 1/2 S_{yz}^{\phi 2} \psi_{2,xy} \right) dA, \end{aligned} \tag{16}$$

where N_{ij}, M_{ij}, $M_{ij}^{\phi\alpha}$, Q_α, Q_α^ϕ, P_{ij}, S_{ij}, $S_{ij}^{\phi\alpha}$ and $A_{ij}^{\phi\alpha}$ are defined as follows

$$\left\{N_{ij}, M_{ij}, M_{ij}^{\phi\alpha}\right\} = \int_{-\frac{h_t}{2}}^{\frac{h_t}{2}} \left\{\sigma_{ij}^k, z\,\sigma_{ij}^k, \phi_\alpha \sigma_{ij}^k\right\} dz, \tag{17a}$$

$$\begin{aligned} &\left\{Q_\alpha, Q_\alpha^\phi\right\} = \int_{-\frac{h_t}{2}}^{\frac{h_t}{2}} \left\{\sigma_{pq}^k, \phi_\alpha^k \sigma_{pq}^k\right\} dz, \\ &\left(p = x, y\ , q = z\right), \end{aligned} \tag{17b}$$

$$L_{1jj} = \int_{-h_1 - \frac{h_m}{2}}^{-\frac{h_m}{2}} D_{jj}^a \sin\left(\pi\left(-z - \frac{h_m}{2}\right) \Big/ h_1\right) dz, \tag{17c}$$

$$L_{2jj} = \int_{\frac{h_m}{2}}^{\frac{h_m}{2} + h_1} D_{jj}^c \sin\left(\pi\left(z - \frac{h_m}{2}\right) \Big/ h_1\right) dz, \tag{17d}$$

$$\left\{P_{ij}, S_{ij}, S_{ij}^{\phi\alpha}, A_{ij}^{\phi\alpha}\right\} = \int_{-\frac{h_t}{2}}^{\frac{h_t}{2}} \left\{m_{ij}^k, z m_{ij}^k, \phi_\alpha^k m_{ij}^k, \phi_{\alpha,z}^k m_{ij}^k\right\} dz, \tag{17e}$$

3.2 External works

The external works exerted to the systems are:

- Two dimensional magnetic field,
- Orthotropic Pasternak foundation,
- External applied voltages,
- Biaxial uniform compressive loads.

3.2.1 Magnetic fields

Core layer of micro structure is composed of CNTs which are sensitive to magnetic field. When a solid structure is affected by a magnetic field, magnetic forces would apply on each element of the structure. Based on Maxwell relations, $(\vec{J})$, current density, $(\vec{h})$, disturbing vectors of magnetic field, $(\vec{e})$, strength vectors of electric field, $(\vec{U})$, the vector of displacement and $(\vec{H})$, magnetic field vector can be written as Narendar *et al*. (2012)

$$\begin{aligned} &\vec{J} = \nabla \times \vec{h},\ \nabla \times \vec{e} = -\eta \dot{\vec{h}},\ \nabla \cdot \vec{h} = 0, \\ &\vec{e} = -\eta\left(\vec{U} \times \vec{H}\right), \vec{h} = \nabla \times \left(\vec{U} \times \vec{H}\right), \end{aligned} \tag{18a}$$

The Lorentz force can be expressed as

$$f_m = \eta\left(\vec{J}\times\vec{H}\right), \tag{18b}$$

where η is the magnetic permeability. In electro-magnetism, permeability is the measure of the ability of a material to support the formation of amagnetic field within itself. Hence, it is the degree of magnetization that a material obtains in response to an applied magnetic field. The magnitudes of the exerted forces mainly rely upon the strength of the applied magnetic field and magnetic permeability of the continuum under study as well as its deformation regime. The SMP is under two-dimensional magnetic field. when magnetic field is imposed along the α-direction, it could be written as $\vec{H} = \vec{H}_x\delta_{x\alpha}e_x + \vec{H}_y\delta_{y\alpha}e_y$, where $\delta_{\beta\alpha}$ is Kronecker delta tensor (α, β = x, y). To expand Eqs. (18) and using Eqs. (10), the Lorentz force terms along the x, y and z directions can be expressed as

$$\begin{aligned} f_x &= \eta H_y^2\left[\left(u_{,xx}+u_{,yy}\right)+z\left(\theta_{1,xx}+\theta_{1,yy}\right)\right. \\ &\left.+\phi_{1b}\left(\psi_{1,xx}+\psi_{1,yy}\right)\right], \end{aligned} \tag{19a}$$

$$\begin{aligned} f_y &= \eta H_x^2\left[\left(v_{,xx}+v_{,yy}\right)+z\left(\theta_{2,xx}+\theta_{2,yy}\right)\right. \\ &\left.+\phi_{2b}\left(\psi_{2,xx}+\psi_{2,yy}\right)\right], \end{aligned} \tag{19b}$$

$$f_z = \eta H_x^2\left(w_{,xx}+\theta_{2,y}\right)+\eta H_y^2\left(w_{,yy}+\theta_{1x}\right), \tag{19c}$$

where H_x and H_y are the terms of magnetic field in x and y directions, respectively. The resultant forces and the bending moments are expressed as follows Ghorbanpour Arani *et al*. (2016)

$$\begin{aligned} &\left\{F_{mi}, M_{mi}, M_{mi}^{\phi\alpha}\right\} = \int_{-\frac{h_m}{2}}^{\frac{h_m}{2}} f_i\left(1, z, \phi_\alpha\right)dz, \\ &(i = x, y, z), \end{aligned} \tag{20}$$

Therefore, the external work due to the magnetic field is obtained as follows

$$\begin{aligned} W_{magnetic} = \int_{-\frac{h_m}{2}}^{\frac{h_m}{2}} &\left(F_{mx}u + F_{my}v + F_{mz}w + M_{mx}\theta_1\right. \\ &+M_{my}\theta_2 + \left(M_{mx}^{\phi 1} + M_{mx}^{\phi 2}\right)\psi_1 \\ &\left.+\left(M_{my}^{\phi 1} + M_{my}^{\phi 2}\right)\psi_2\right)dz. \end{aligned} \tag{21}$$

3.2.2 Orthotropic Pasternak foundation

The external work exerted to the SMP from surrounding elastic medium can be expressed as Ghorbanpour Arani *et al*. (2016)

$$\begin{aligned} W_P = \frac{1}{2}\int_A &\left(k_w w - k_{gx}\left(\left(\cos^2\theta\right)w_{,xx}\right.\right. \\ &+2\sin\theta\cos\theta w_{,xy}+\left(\sin^2\theta\right)w_{,yy}\Big) \\ &-k_{gy}\left(\left(\sin^2\theta\right)w_{,xx}-2\sin\theta\cos\theta w_{,xy}\right. \\ &\left.\left.+\left(\cos^2\theta\right)w_{,yy}\right)wdA, \end{aligned} \tag{22}$$

in which k_w presents the spring constant of Winkler type, k_{gx} and k_{gy} are shear foundation parameters in ξ and in η direction, respectively.

3.2.3 Electric and mechanic forces

N_{xe}, N_{ye} and N_{xm}, N_{ym} describe electric forces and uniform compressive loadings along x – and y – axes, respectively and can be written as follows

$$N_{xe} = e_{31}^{a,c}\int_{-\frac{h_1}{2}}^{\frac{h_1}{2}} E_{zz}dz,\ N_{ye} = e_{32}^{a,c}\int_{-\frac{h_1}{2}}^{\frac{h_1}{2}} E_{zz}dz, \tag{23a}$$

$$N_{xm} = -N,\quad N_{ym} = -k_0 N, \tag{23b}$$

in which k_0 is the load factor, V_1 and V_2 indicate the external applied voltages of lower and upper layers, respectively. Therefore, the external work due to external applied voltages and compressive loads can be written as follows

$$\begin{aligned} W_{EM} = \frac{1}{2}\int_A &\left(\left(N_{xm}+N_{xe}\right)w_{,xx}\right. \\ &\left.+\left(N_{ym}+N_{ye}\right)w_{,yy}\right)wdA, \end{aligned} \tag{24}$$

3.3 Kinetic energy

The total kinetic energy of SMP may be defined as

$$\begin{aligned} K = \frac{1}{2}\rho^k\int_{-\frac{h_t}{2}}^{\frac{h_t}{2}}\int_A &\left\{\left(\left(\dot{U}_1^k\right)^2+\left(\dot{V}_1^k\right)^2\right.\right. \\ &\left.\left.+\left(\dot{W}_1^k\right)^2 dA\right\}dz. \end{aligned} \tag{25}$$

Using Hamilton's principle and substituting Eqs. (15), (21), (22), (24) and (25) into Eq. (14) the governing equations of motion can be expressed as

$$\begin{aligned} \delta u:\ &N_{xx,x}+N_{xy,y}+1/2P_{yz,yy}+1/2P_{xz,xy} = \\ &+I_0\ddot{u}+I_1\ddot{\theta}_1+\rho^a K_1\ddot{\psi}_1+\rho^b K_3\ddot{\psi}_1 \\ &+\rho^c K_5\ddot{\psi}_1 - F_{mx}, \end{aligned} \tag{26a}$$

$$\begin{aligned} \delta v:\ &N_{yy,y}+N_{xy,x}-1/2P_{yz,xy}-1/2P_{xz,xx} = \\ &+I_0\ddot{v}+I_1\ddot{\theta}_2+\rho^a K_2\ddot{\psi}_2+\rho^b K_4\ddot{\psi}_2 \\ &+\rho^c K_6\ddot{\psi}_2 - F_{my}, \end{aligned} \tag{26b}$$

$$\begin{aligned} \delta w:\ &Q_{2,y}+Q_{1,x}-1/2P_{xx,xy}+1/2P_{xy,xx} \\ &-1/2P_{xy,yy}+1/2P_{yy,xy} = I_0\ddot{w}+W_P \\ &+W_{EM}-F_{mz}, \end{aligned} \tag{26c}$$

$$\begin{aligned} \delta\theta_1:\ &M_{xx,x}+M_{xy,y}-Q_1+1/2S_{yz,yy}+1/2S_{xz,xy} \\ &+1/2P_{xy,x}-1/2P_{zz,y}+1/2P_{yy,y} = I_1\ddot{u} \\ &+I_2\ddot{\theta}_1+\rho^a B_1\ddot{\psi}_1+\rho^b B_3\ddot{\psi}_1+\rho^c B_5\ddot{\psi}_1 - M_{mx}, \end{aligned} \tag{26d}$$

$$\begin{aligned} \delta\theta_2:\ &M_{yy,y}+M_{xy,x}-Q_2-1/2S_{yz,xy}-1/2S_{xz,xx} \\ &-1/2P_{xy,y}+1/2P_{zz,x}-1/2P_{xx,x} = I_2\ddot{\theta}_2 \\ &+I_1\ddot{v}+\rho^a B_2\ddot{\psi}_2+\rho^b B_4\ddot{\psi}_2+\rho^c B_6\ddot{\psi}_2 - M_{my}, \end{aligned} \tag{26e}$$

$$\begin{aligned}\delta\psi_1:\ & M^{\phi 1}_{xx,x}+M^{\phi 1}_{xy,y}-Q^{\phi}_{1}+1/2A^{\phi 1}_{xy,x}\\ & -1/2A^{\phi 1}_{zz,y}+1/2A^{\phi 1}_{yy,y}+1/2S^{\phi 1}_{xz,xy}\\ & +1/2S^{\phi 1}_{yz,y}=\rho^a K_1\ddot{u}+\rho^b K_3\ddot{u}+\rho^c K_5\ddot{u}\\ & +\rho^a B_1\ddot{\theta}_1+\rho^c B_5\ddot{\theta}_1+\rho^c E_{55}\ddot{\psi}_1+\rho^b E_{33}\ddot{\psi}_1\\ & +\rho^b B_3\ddot{\theta}_1+\rho^a E_{11}\ddot{\psi}_1-M^{m\phi}_{1x}-M^{m\phi}_{2x},\end{aligned} \tag{26f}$$

$$\begin{aligned}\delta\psi_2:\ & M^{\phi 2}_{xy,x}+M^{\phi 2}_{yy,y}-Q^{\phi}_{2}-1/2A^{\phi 2}_{xx,x}-1/2S^{\phi 2}_{xz,xx}\\ & -1/2S^{\phi 2}_{yz,xy}-1/2A^{\phi 2}_{xy,y}+1/2A^{\phi 2}_{zz,x}=\rho^a B_2\ddot{\theta}_2\\ & +\rho^b B_4\ddot{\theta}_2+\rho^c B_6\ddot{\theta}_2+\rho^a E_{22}\ddot{\psi}_2+\rho^b E_{44}\ddot{\psi}_2\\ & +\rho^c E_{66}\ddot{\psi}_2+\rho^a K_2\ddot{v}+\rho^b K_4\ddot{v}+\rho^c K_6\ddot{v}\\ & -M^{m\phi}_{1y}-M^{m\phi}_{2y},\end{aligned} \tag{26g}$$

$$\delta\varphi_1:\ L_{xx,x}+L_{yy,y}+\pi L_{zz}/h_1=0, \tag{26h}$$

$$\delta\varphi_2:\ L_{2xx,x}+L_{2yy,y}-\pi L_{2zz}/h_1=0, \tag{26i}$$

where I_0, I_1 and I_2 define the mass moments of inertia of k^{th} layer and can be written as

$$\begin{aligned}I_0 &= \int_{-\frac{h_t}{2}}^{\frac{h_t}{2}}\rho^k dz \quad , I_1=\int_{\frac{h_t}{2}}^{\frac{h_t}{2}}\rho^k z dz,\\ I_2 &= \int_{\frac{h_t}{2}}^{\frac{h_t}{2}}\rho^k z^2 dz,\end{aligned} \tag{27}$$

The simply supported mechanical and electrical boundary conditions can be expressed as

$$x=0,a\rightarrow\begin{cases}v=w=\theta_2=\psi_2=\varphi_2=0,\\ N_{xx}=M_{xx}=M^{\phi 1}_{xx}=L_{1xx}=0,\end{cases} \tag{28a}$$

$$y=0,b\rightarrow\begin{cases}u=w=\theta_1=\psi_1=\varphi_1=0,\\ N_{yy}=M_{yy}=M^{\phi 2}_{yy}=L_{2yy}=0.\end{cases} \tag{28b}$$

Other parameters in Eqs. (26) are defined in Appendix A. It is convenient to define the following dimensionless parameters as

$$\begin{aligned}&X=\frac{x}{a},Y=\frac{y}{b},(U,V,W)=\frac{(u,v,w)}{h_m},,\overline{\varphi}_k=\frac{\varphi}{\varphi_\alpha}\\ &A_\alpha=\frac{V_\alpha}{\varphi^k_\alpha},\theta_i=\overline{\theta}_i,\psi_i=\overline{\psi}_i,\varphi_\alpha=h_m\sqrt{\frac{Q_{k11}}{\mu^k_{11}}},\\ &\left(\overline{Q_{k12}},\overline{Q_{k22}},\overline{Q_{k44}},\overline{Q_{k55}},\overline{Q_{k66}}\right)=\frac{Q^k_{12},Q^k_{22},Q^k_{44},Q^k_{55},Q^k_{66}}{Q_{a11}},\\ &\left(E^k_{15},E^k_{24},E^k_{31},E^k_{32}\right)=\frac{\left(e^k_{15},e^k_{24},e^k_{31},e^k_{32}\right)}{\sqrt{Q_{a11}}\sqrt{\mu^k_{11}}},\overline{B_i}=\frac{B_i}{b^3},\\ &\overline{P}^{\beta i}_{sc,a}=\frac{R^{\beta i}_{sc,a}}{a},\tau=\frac{t}{h_m}\sqrt{\frac{Q^a_{11}}{\rho^a}},\overline{F_i}=\frac{F_i}{a},\overline{p_i}=\frac{p_i}{b^3},\\ &\overline{k_{gx}}=\frac{k_{gx}}{Q_{a11}a},\overline{k_{gy}}=\frac{k_{gy}}{Q_{a11}a},L=\frac{l}{a},\overline{K_i}=\frac{K_i}{a^2},\end{aligned} \tag{29}$$

$$\begin{aligned}&\overline{P}^{a,c}_{ai}=\frac{P^{a,c}_{ai}}{a},\overline{T}^{a,c}_{ai}=\frac{T^{a,c}_{ai}}{b^2}N^*=\frac{Nb^2}{Q_{a11}h^3_m},\\ &\overline{k_w}=\frac{k_w h_m}{Q_{a11}},\overline{C_{k44}}=\frac{Q_{k44}l^2}{a^2},\overline{L}_{i\alpha\alpha}=\frac{L_{i\alpha\alpha}}{a\sqrt{Q_{a11}}\sqrt{\mu^a_{11}}}\\ &\left(\alpha_{ab},\alpha_{mb},\alpha_{ba},\alpha_m,\alpha_{bm}\right)=\left(\frac{a}{b},\frac{h_m}{b},\frac{b}{a},\frac{h_1}{h_m},\frac{b}{h_m}\right),\end{aligned} \tag{29}$$

Substituting Eqs. (17) into Eqs. (26) and using Eq. (29) yields the dimensionless governing equations.

4. Solution method

In the present manuscript, an analytical solution is selected to obtain free vibration and buckling responses of simply supported SMP are obtained separately based on the MCST.

4.1 Free vibration response

The displacements are expanded in double Fourier series based on Navier solution for simply supported end conditions as follows Iurlaro *et al*. (2013)

$$\begin{Bmatrix}U\\ \overline{\theta}_1\\ \overline{\psi}_1\end{Bmatrix}=\sum_{m=1}^{\infty}\sum_{n=1}^{\infty}\begin{Bmatrix}U_{mn}\\ \Lambda^1_{mn}\\ \Psi^1_{mn}\end{Bmatrix}\cos(m\pi X)\sin(n\pi Y)e^{i\omega\tau}, \tag{30a}$$

$$\begin{Bmatrix}V\\ \overline{\theta}_2\\ \overline{\psi}_2\end{Bmatrix}=\sum_{m=1}^{\infty}\sum_{n=1}^{\infty}\begin{Bmatrix}V_{mn}\\ \Lambda^1_{mn}\\ \Psi^1_{mn}\end{Bmatrix}\sin(m\pi X)\cos(n\pi Y)e^{i\omega\tau}, \tag{30b}$$

$$\begin{Bmatrix}W\\ \overline{\varphi}_1\\ \overline{\varphi}_2\end{Bmatrix}=\sum_{m=1}^{\infty}\sum_{n=1}^{\infty}\begin{Bmatrix}W_{mn}\\ \Pi^1_{mn}\\ \Pi^2_{mn}\end{Bmatrix}\sin(m\pi X)\sin(n\pi Y)e^{i\omega\tau}, \tag{30c}$$

in which n and m are half wave numbers, $\Omega=\{U_{mn}, V_{mn}, W_{mn}, \Lambda^1_{mn}, \Lambda^2_{mn}, \Psi^1_{mn}, \Psi^2_{mn}, \Pi^1_{mn}, \Pi^2_{mn}\}$ are the amplitude constants, ω is the dimensionless natural frequency and $i=\sqrt{-1}$. Inserting Eqs. (30) into dimensionless governing equations, the following relation can be concluded

$$\det\left(\left[K\right]-\omega^2\left[M\right]\right)=0, \tag{31}$$

where [K] is the stiffness matrix and [M] is the mass matrix. Finally, the dimensionless frequency of the system can be calculated from Eq. (31).

4.2 Buckling response

Similarly, the buckling response of the SMP can be obtained using Navier method by neglecting the time harmonic factors in Eqs. (26) and (30). Therefore, in order to obtain the critical buckling loads the following equations are solved

$$\det\left(\left[K\right]\{\Omega\}\right)=0. \tag{32}$$

Table 1 Material properties of MEE layers

CNT & Matrix	ZnO	
$E_{11}^{cnt} = 5.6466$ (TPa)	$Q_{11} = 207$ (GPa)	$e_{31} = -0.51\ (C/m^2)$
	$Q_{12} = 117.7$ (GPa)	$e_{32} = -0.51\ (C/m^2)$
	$Q_{13} = 106.1$ (GPa)	$e_{33} = 1.22\ (C/m^2)$
	$Q_{22} = 207$ (GPa)	$e_{15} = -0.45\ (C/m^2)$
	$Q_{23} = 106.1$ (GPa)	$e_{24} = -0.45\ (C/m^2)$
	$Q_{33} = 209.5$ (GPa)	$\epsilon_{11} = 7.77 \times 10^{-8}\ (F/m^2)$
$\eta_1 = 0.149$	$Q_{44} = 44.8$ (GPa)	$\epsilon_{22} = 7.77 \times 10^{-8}\ (F/m)$
$\eta_2 = \eta_3 = 0.934$	$Q_{55} = Q_{66} = 44.6$ (GPa)	$\epsilon_{33} = 8.91 \times 10^{-8}\ (F/m)$

Table 2 Comparison of uniaxial buckling load parameter, $N^* = \frac{Nb^2}{Q_{a11}h_m^3}$

l/h_l	FSDT			RZT
	$k_x^2 = k_y^2 = 1$	$k_x^2 = k_y^2 = 5/6$	$k_x^2 = k_y^2 = 2/3$	
0.5	2.6629	2.5393	2.4024	1.8021
0.6	2.8321	2.7002	2.5537	1.9965
0.7	3.0231	2.8816	2.7245	2.2233
0.8	3.2337	3.0816	2.9130	2.4813
0.9	3.4620	3.2986	3.1180	2.7684
1.0	3.7066	3.5313	3.3383	3.0824

Table 3 Comparison of critical buckling load between present results

Method	h_m/a		
	0.05	0.1	0.2
Hosseini-Hashemi *et al*. (2008)	3.9444	3.7864	3.2637
Shufrin and Eisenberger (2005)	-	3.7865	3.2637
Mizusawa (1993)	3.944	3.784	3.256
Present work (RZT)	3.7379	3.5168	3.0277

5. Numerical results and discussion

In this section, the effects of FG distributions and volume fraction of CNTs, aspect ratio, surrounding elastic medium, external applied voltages, small scale parameter, magnetic field, load factor and mode numbers on the critical buckling loads and natural frequency of the SMP are studied in detail. ZnO is selected for the piezoelectric layers. It is supposed that the magnetic permeability of SWCNTs equals the magnetic permeability of the medium around it, $\eta = 4\pi \times 10^{-7}$ (Hosseini and Sadeghi-Goughari 2015). The effective material properties of matrix polymer, SWCNT and ZnO are presented in Table 1 (Alibeigloo 2013, Ghorbanpour Arani *et al*. 2016).

In order to show the accuracy of the results obtained based on RZT, the uniaxial critical buckling load of the SMP are compared with those obtained based on first order shear deformation theory (FSDT) for different values of shear correction factors k_x^2 and k_y^2 in Table 2. It is demonstrated in Table 2 that increasing the values of shear correction factors decreases the uniaxial buckling load factor based on FSDT and results obtained based on FSDT become close to those obtained using RZT.

Table 4 Validation of the present work with Ref. Lei *et al*. (2012) for dimensionless buckling load

Method	Load factors ($k_0 = -1$, $k_1 = -1$)	
	Dimensionless buckling load Lei *et al*. (2012)	Dimensionless load buckling (present)
UD	5.8831	5.3619
FG-X	6.4384	5.8910
FG-O	4.8946	4.4785

Table 5 Validation of present work with Lei *et al*. (2012) for dimensionless buckling load

Method	Load factors ($k_0 = -1$, $k_1 = +1$)	
	Dimensionless buckling load Lei *et al*. (2012)	Dimensionless load buckling (present)
UD	28.4768	27.8558
FG-X	29.1897	28.5080
FG-O	24.0474	23.4030

To the best of the author's knowledge no published paper is available for buckling and free vibration analysis of embedded FG-CNTRC micro plate integrated with ZnO layers. Therefore, in an attempt to validate this research, a simplified analysis of this paper is compared with results obtained by Ref. (Hosseini-Hashemi *et al*. 2008 and Mizusawa 1993). The comparison is shown in Table 3. It is seen from Table 3 that the present results are in a good agreement in comparison with results obtained by Ref. (Hosseini-Hashemi *et al*. 2008 and Mizusawa 1993).

In another attempt to validate the results of this investigation, a FG-CNTRC plate using Ritz method Lei *et al*. (2012). The theory used in this paper is FSDT and the amount of critical buckling load for diferrent distributions of CNTs are compared and for various load factors. The comparisons are shown in Tables 4-5. It is obvious from Tables 4-5 that the present results are in a good agreement in comparison with results obtained by Ref. (Lei *et al*. 2012).

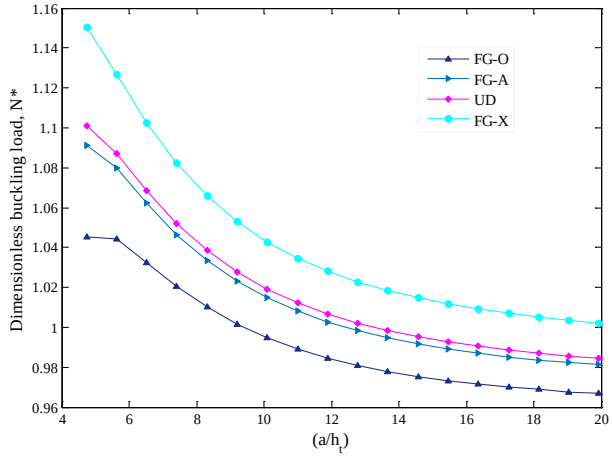

Fig. 2 Effect the FG distribution of CNTs on the dimensionless critical buckling mechanical load

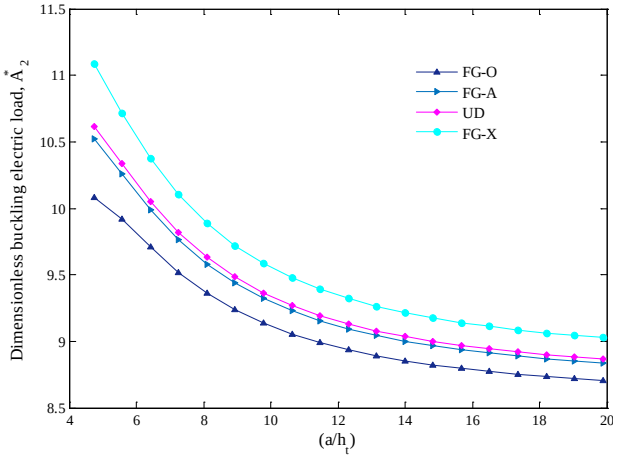

Fig. 3 Effect the FG distribution of CNTs on the dimensionless critical buckling electric load

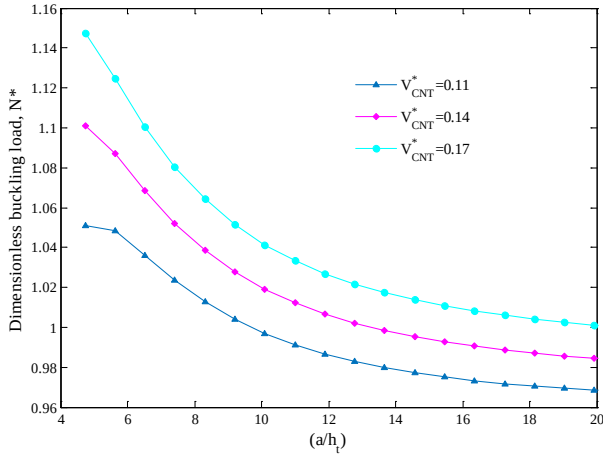

(a) Dimensionless critical buckling mechanical load

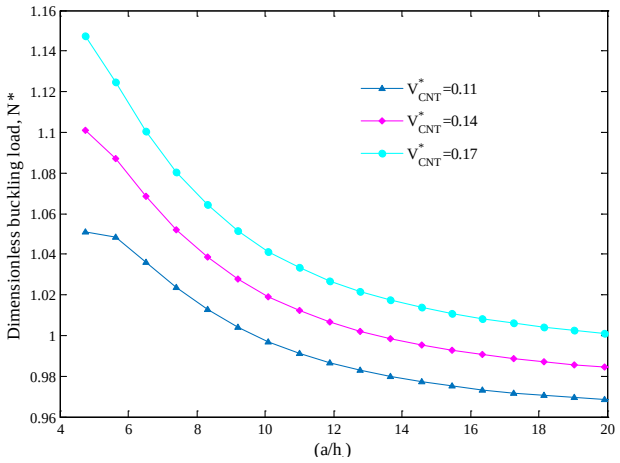

(b) Dimensionless critical buckling electric load

Fig. 4 Effect of CNTs volume fraction versus aspect ratio of the length to thickness (a/h_t)

5.1 Buckling analysis

Figs. 2 and 3 depict the effect of different types of FG distribution of CNTs on the critical buckling mechanical and electric loads, respectively, versus aspect ratio of the length to thickness of the SMP. As can be seen, the $FG-X$ distribution of CNTs results higher critical buckling loads. This is due to the fact that the in $FG-X$ distribution, SWCNTs are close to the top and bottom of the core layer. Therefore, the stiffness of the sandwich micro plate increases. It should be noticed, the results of *UD* and $FG-\Lambda$ types are close to each other and $FG-O$ distribution has the least effect on the critical buckling loads, consequently. Furthermore, it can be seen from Fig. 2 that increasing the aspect ratio of length to the thickness of SMP, decreases the critical buckling mechanic and electric loads. It should be noticed, $V_{CNT}^{*} = 0.17$, $1/h_t = 1$, $a/b = 1.5$ and $h_1/h_m = 0.05$ are assumed in these figures. In fact, increasing the aspect ratio of length to the thickness make the structure looser.

The variation of critical buckling mechanical and electric loads for different CNTs volume fraction versus aspect ratio of length to thickness, are shown in Figs. 4(a)-(b), respectively. It is seen from Fig. 4(a) that increasing CNTs volume fraction, increases critical buckling loads. It is because increasing the volume fraction of CNTs increases the stiffness of the structure. Moreover, the CNTs volume fraction is more effective on critical buckling mechanic load than electric load.

Fig. 5 shows the effect of four cases of elastic mediums including neglecting foundation, Winkler, Pasternak and orthotropic Pasternak foundations, on the critical buckling mechanical load with respect to aspect ratio and length to thickness ratio, respectively. The following data are assumed to plot Figs. 4(a) and (b): $k_w = 30\times10^{12}$ (N/m^3), $k_g = 80$ (N/m), $k_{gx} = 90$ (N/m), $k_{gy} = 80$ (N/m) and $\theta = 45°$. It can be observed that considering elastic medium increase the critical buckling loads of SMP. This is due to this fact that considering elastic medium makes the structure stiffer. Moreover, the effect of Pasternak foundation is more considerable than Winkler foundation in increasing the critical buckling loads. Because Pasternak foundation assumes both shear and normal loads while Winkler foundation just assumes normal loads. Also, orthotropic Pasternak foundation is more effective than Pasternak

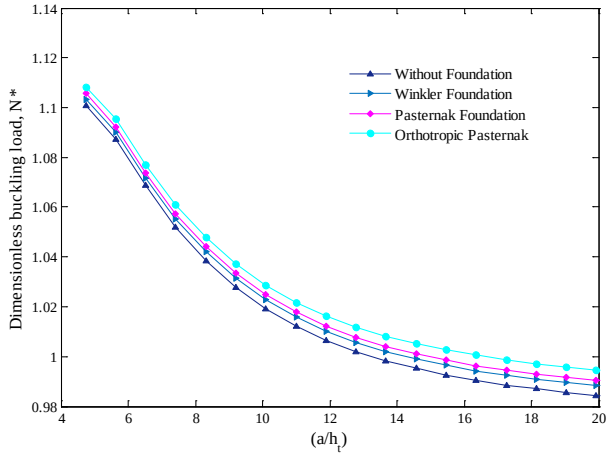

Fig. 5 Effect of elastic medium on the dimensionless critical buckling mechanical load versus aspect ratio of the length to thickness (a/h_t)

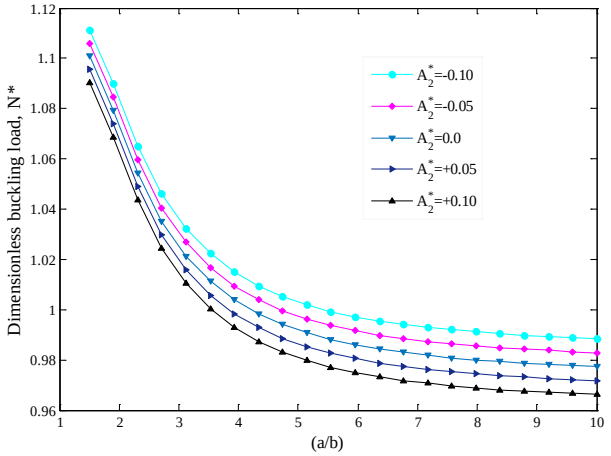

Fig. 7 Effect of external applied voltages versus aspect ratio of length to width (a/b) on the dimensionless critical buckling mechanical load

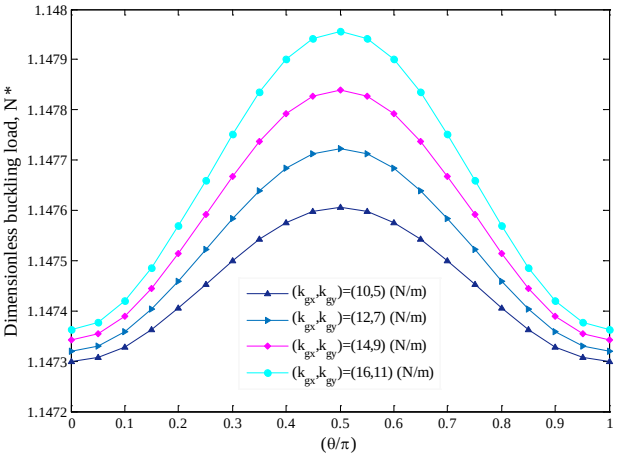

Fig. 6 Dimensionless critical buckling load versus orthotropy angle of elastic medium

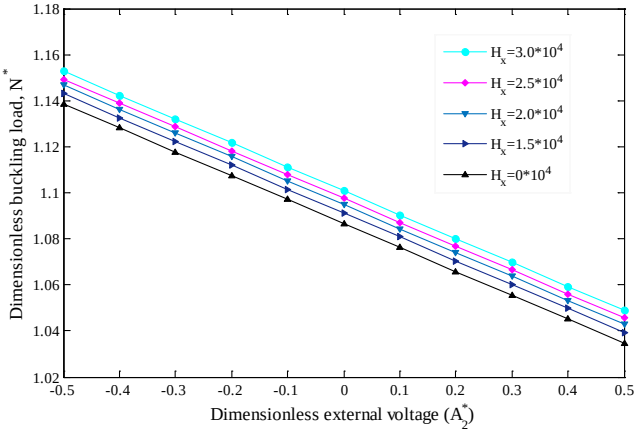

Fig. 8 Effect of both external applied voltage and magnetic field along x- direction on the dimensionless critical buckling mechanical load

foundation to increases critical buckling loads. In fact, orthotropic Pasternak foundation estimates a stiffer structure than others. Moreover, the effect of elastic medium on the critical buckling loads are more visible for higher aspect ratio of length to the thickness ratio values.

In order to show the effect of surrounding elastic medium completely, Fig. 6 is plotted to find out the effects of orthotropic foundation on critical buckling mechanical load versus orthotropy angle for different Pasternak shear constants. As observed from Fig. 6 and due to the Eq. (22), assuming $\theta = 90°$ yields the dimensionless critical buckling load at its maximum value. It is due to the fact that orthotropic Pasternak model considers not only the normal stresses but also the transverse shear deformation and continuity among the spring elements. In this section, $V_{CNT}^{*} = 0.17$, $1/h_t = 1$, $a/b = 1.5$ and $h_1/h_m = 0.05$ are hypothesized.

Dimensionless critical buckling mechanical load according to different amount of dimensionless external applied voltages versus aspect ratio of length to width of the SMP are shown in Fig. 7. As can be seen, imposing applied voltages from negative to positive values, decreases the critical buckling loads. Indeed, imposing positive and negative external voltages generate axial compressive and tensile forces on the bottom and top of the SMP, respectively. Therefore, the applied external voltage is an effective controlling parameter for buckling of the system. Furthermore, the effect of external applied voltages on the critical buckling loads becomes more distinguished at higher aspect ratio of length to width values. Volume fraction of CNTs, thickness ratio, aspect ratio and load factor assumed in this figure are respectively 0.14, 0.05, 1.5 and 0.8.

In order to reveal the effect of coupling between electric and magnetic fields and the use of these parameters to control the mechanical behaviors of SMP, Fig. 8 is plotted. As can be seen, increasing the external voltage, decreases the dimensionless critical buckling load. Increasing magnetic field along x- direction causes enhances the dimensionless critical buckling mechanical load. This is due to this fact that the magnetic field creates a force to the structure. In Fig. 8, $1/h_t = 1$, $V_{CNT}^{*} = 0.14$, $a/b = 1.5$ and $h_1/h_m = 0.05$ are supposed and foundation parameters are assumed zero.

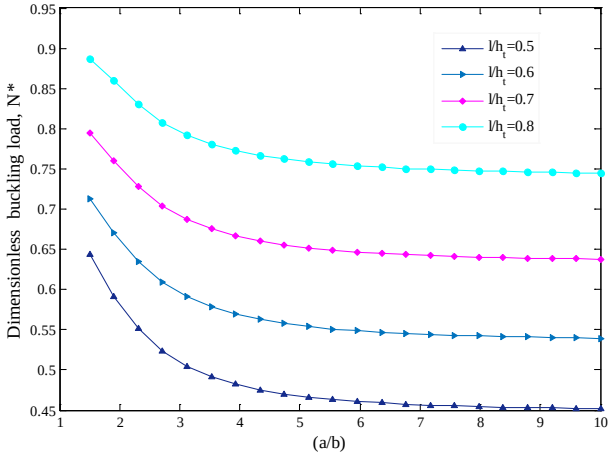

Fig. 9 Effect of small scale parameter versus aspect ratio of length to width (a/b) on the dimensionless critical buckling mechanical load

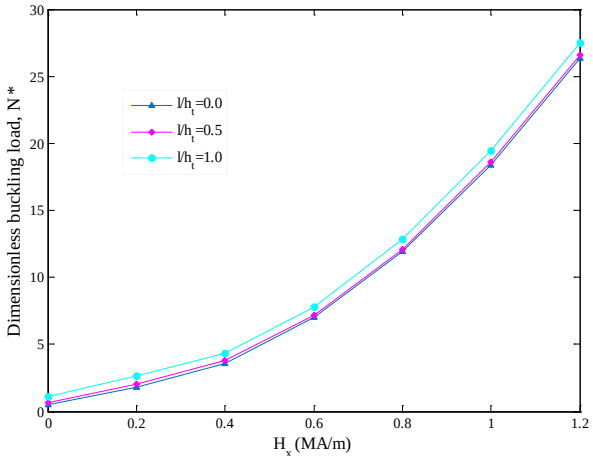

Fig. 10 Effect of small scale parameter on the dimensionless critical buckling electric load versus magnetic field (H_x)

Fig. 9 represents the effects of small scale parameter (l) on the critical buckling mechanical load with respect to the aspect ratio of length to width, respectively. It is shown that, by increasing small scale parameter values, the critical buckling loads increases. It is due to the fact that according to Eq. (6), increasing the small scale parameter increases the total strain energy of the SMP. Moreover, the small scale parameter is more effective at higher aspect ratio of length to width values. Meanwhile, $V_{CNT}^{*} = 0.17$, $k_0 = 0.8$, $a/b = 1.5$ and $h_1/h_m = 0.05$ and foundation coefficients are assumed zero.

Dimensionless critical buckling mechanical load versus magnetic field along x- direction is presented in Fig. 10. It can be concluded that, as the structure is subjected to magnetic field, the critical buckling load increases. Because imposing magnetic field in x-direction creates a force to structure and results higher critical buckling loads. It can be understood that applying magnetic field is more effective than other controlling parameters. In this figure, $k_0 = 0.8$, $1/h_t = 1$, $V_{CNT}^{*} = 0.14$, and $a/b = 1.5$.

Effects of mode numbers on the dimensionless critical buckling mechanic load are also illustrated in Fig. 11.

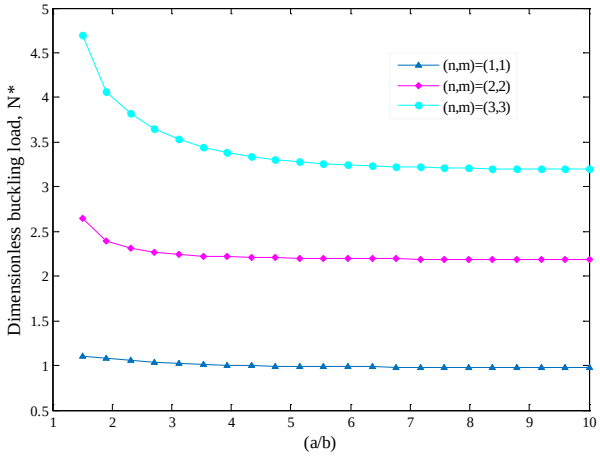

Fig. 11 Effect of mode numbers on the dimensionless critical buckling mechanic load

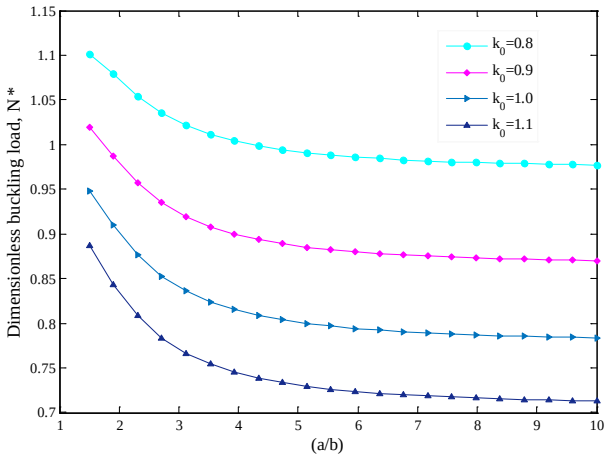

Fig. 12 Effect of load factor on the dimensionless critical buckling mechanical load

As can be seen from Fig. 11, the critical buckling load increase as the mode numbers are increased.

Finally, Fig. 11 shows the effect of load factor (k_0) on the critical buckling mechanic load versus the aspect ratio of length to width. It is seen from Fig. 12 that with increasing the load factor the critical buckling load decreases. Because with increasing load factor, the compressive uniform load increases.

5.2 Free vibration analysis

Fig. 13 illustrates the influences of magnetic field intensity along x- and y- directions on the dimensionless natural frequency with respect to the aspect ratio of length to thickness, respectively. As can be seen from Figs. 13 and 14, increasing magnetic field intensity along both x- and y- directions, make the system stiffer and that leads to increase the natural frequency, consequently. Also, the effect of magnetic field along both x- and y- directions is more distinguished at lower aspect ratio values. Moreover, comparing Figs. 13 and 14 show that the magnetic field along y- direction is more effective on the natural frequency

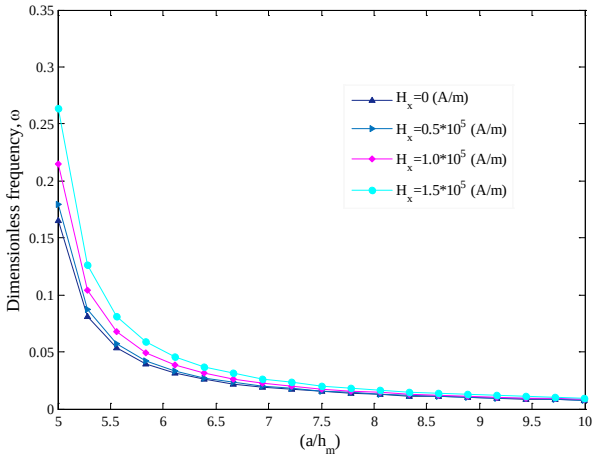

Fig. 13 Effect of magnetic field along *x*- direction on the dimensionless natural frequency versus aspect ratio of the length to core thickness (a/h_m)

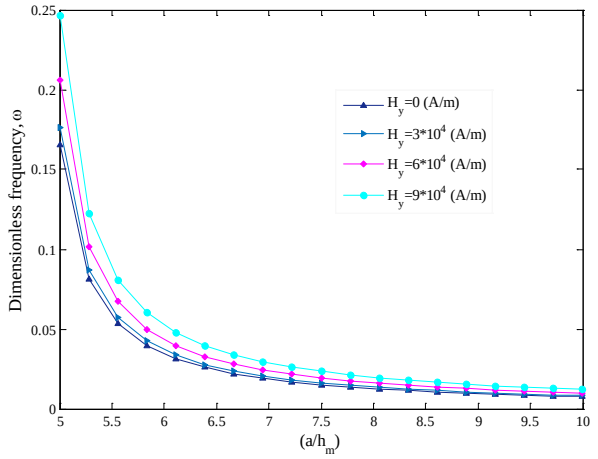

Fig. 14 Effect of magnetic field along *y*- direction on the dimensionless natural frequency

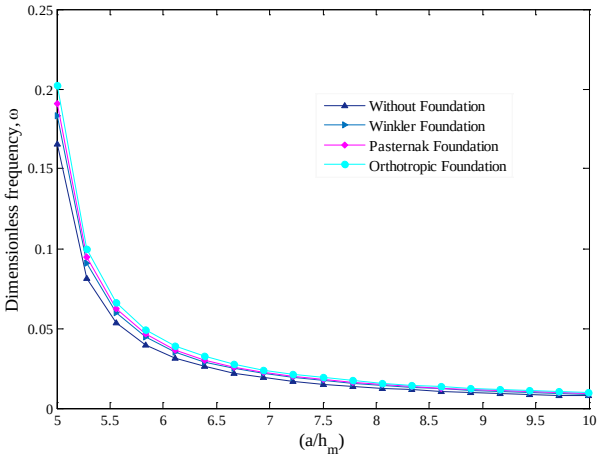

Fig. 15 Effect of elastic medium on the dimensionless natural frequency versus length -thickness (a/h_m)

of the system. In fact, magnetic field can be used as a controlling parameter on the natural frequency. The amount of $1/h_t = 1$, $V_{CNT}^* = 0.14$, $a/b = 1.5$ and $h_1/h_m = 0.05$ are considered and external voltage is zero.

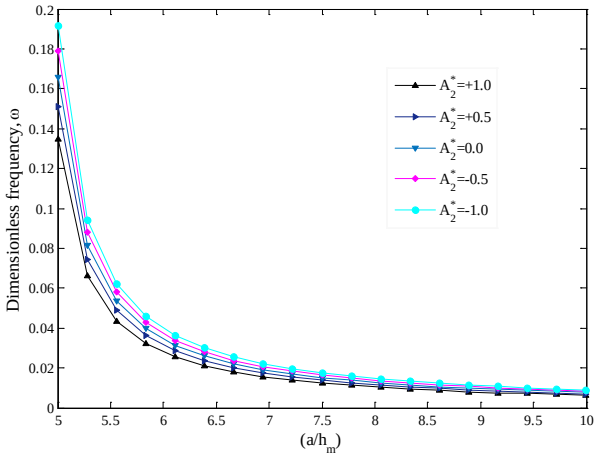

Fig. 16 Effect of external applied voltage on the dimensionless natural frequency versus length-thickness (a/h_m)

The effect of surrounding elastic medium on the dimensionless natural frequency is shown in Fig. 15. It can be understood considering elastic medium increases natural frequency. Because elastic medium make the structure stiffer. Furthermore, it is seen from Fig. 15 that the orthotropic Pasternak foundation is more effective than Winkler and Pasternak ones. It is due to the fact that orthotropic Pasternak elastic medium predicts stiffer structure than others. The following data are supposed to depict Fig. 14: k_w = 30×10^{12} (N/m^3), k_g = 550 (N/m), k_{gx} = 500 (N/m), k_{gy} = 650 (N/m), θ = 90°, $1/h_t = 1$, $V_{CNT}^* = 0.14$, $a/b = 1.5$, $h_1/h_m = 0.05$ and electro-magnetic field's are neglected.

Fig. 16 presents the effect of dimensionless external applied voltage on the dimensionless natural frequency. Imposing positive values of external applied voltage decreases the natural frequency of the SMP. Indeed, imposing positive and negative external voltage values generates axial compressive and tensile forces on the bottom layer of the structure, respectively. In fact, this parameter is useful to control the natural frequency of the system, too. In this figure, $1/h_t = 1$, $V_{CNT}^* = 0.14$, $a/b = 1.5$, $h_1/h_m = 0.05$ are assumed and foundation

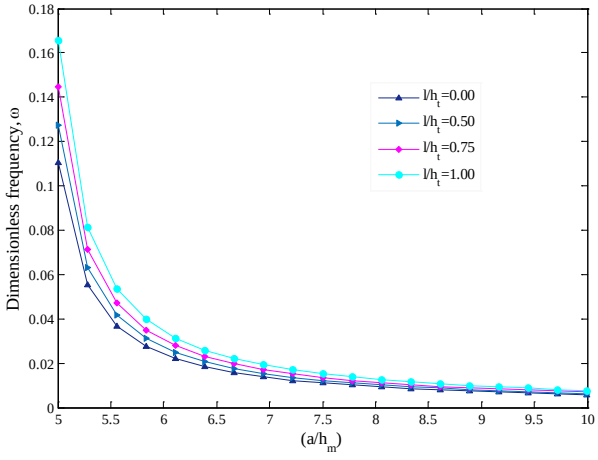

Fig. 17 Effect of small scale parameter on the dimensionless natural frequency versus length-thickness (a/h_m)

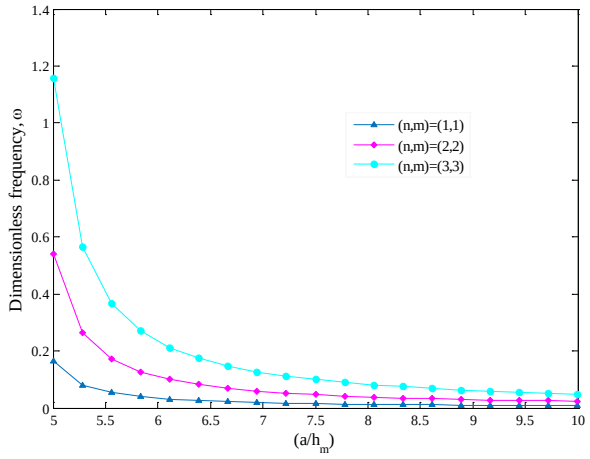

Fig. 18 Effect of mode numbers on natural frequency

coefficients are hypothesized zero.

The effect of small scale parameter on the natural frequency is illustrated in Fig 17. Increasing small scale parameter increases the natural frequency of the SMP. It is due to the fact that according to Eq. (6), the total strain energy increases with increasing small scale parameter. Also, as the aspect ratio of length to core thickness increases, the small scale parameter losses its effect. It should be noticed, $1/h_t = 1$, $V_{CNT}^{*} = 0.14$, $a/b = 1.5$, $h_1/h_m = 0.05$ are considered and foundation coefficients are hypothesized zero.

Effects of mode numbers on the dimensionless natural frequency versus the aspect ratio of length to core thickness are also shown in Fig. 18.

As can be seen from Fig. 18 the natural frequency increase as the mode numbers are increased.

6. Conclusions

Size dependent buckling and free vibration analysis of FG-CNTRC micro plate integrated with ZnO actuator layers was investigated, for the first time in this study. The SMP embedded in orthotropic Pasternak foundation, was subjected to electro-magnetic. To obtain the accurate results, the RZT as well as MSCT were taken into account. Hamilton's principle and energy method were employed to derive governing motion equations. Using an analytical solution the buckling and free vibration responses of the systems were obtained. The obtained results demonstrated that, orthotropic Pasternak elastic medium predicts stiffer structure and therefore higher critical buckling loads and natural frequency values. Moreover, $FG-X$ and $FG-O$ distributions of CNTs in SMPs, has the most and least stiffness between the other types, respectively. Meanwhile, with increasing the CNTs volume fraction, the critical buckling loads and natural frequency increases. 2D magnetic field intensity and external applied voltages are the two important effective parameter to control the mechanical behavior of the system; increasing magnetic fields increases critical buckling loads and natural frequency. Also, since positive and negative voltages generates compressive and tensile forces, therefore, imposing positive voltage values decreases the natural frequency of the SMP. Finally, it is hoped that the obtained results would be beneficial in design of NEMS and MEMS.

Acknowledgments

The author would like to thank the reviewers for their comments and suggestions to improve the clarity of this article. This work was supported by University of Kashan [Grant Number 574600/37].

References

Alibeigloo, A. (2013), "Static analysis of functionally graded carbon nanotube-reinforced composite plate embedded in piezoelectric layers by using theory of elasticity", *Compos. Struct.*, **95**, 612-622.

Esawi, A.M.K. and Farag, M.M. (2007), "Carbon nanotube reinforced composites: Potential and current challenge", *Mater. Design.*, **28**(9), 2394-2401.

Ferreira, A.J.M., Fasshauer, G.E., Batra, R.C. and Rodrigues, J.D. (2008), "Static deformations and vibration analysis of composite and sandwich plates using a layerwise theory and RBF-PS discretizations with optimal shape parameter", *Compos. Struct .*, **86**(4), 328-343.

Fiedler, B., Gojny, F.H., Wichmann, M.H.G., Nolte, M.C.M. and Schulte, K. (2006), "Fundamental aspects of nano-reinforced composites", *Compos. Sci. Technol.*, **66**(16), 3115-3125.

Ghorbanpour Arani, A., Abdollahian, M. and Jalaei, M.H. (2015a), "Vibration of bioliquid-filled microtubules embeded in cytoplasm including surface effects using modified couple stress theory", *J. Theor. Biol.*, **367**, 29-38.

Ghorbanpour Arani, A., Kolahchi, R. and Zarei, M.s. (2015b), "Visco-surface-nonlocal piezoelasticity effects on nonlinear dynamic stability of graphene sheets integrated with ZnO sensor and actuators using refined Zigzag theory", *Compos. Struct.*, **132**, 506-526.

Ghorbanpour Arani, A., Mosayyebi, M., Kolahdouzan, F., Kolahchi R. and Jamali, M. (2016), "Refined Zigzag theory for vibration analysis of viscoelastic FG-CNTRC micro plates integrated with piezoelectric layers", *P. I. Mech. Eng G-J Aer.* DOI: 10.1177/0954410016667150

Hosseini, M. and Sadeghi-Goughari, M. (2016), "Vibration and instability analysis of nanotubes conveying fluid subjectrd to a longitudinal magnetic field", *App. Math. Model.*, **40**(4), 2560-2576.

Hosseini-Hashemi, S.H., Khorshidi, K. and Amabili, M. (2008), "Exact solution for linear buckling of rectangular Mindlin plates", *J. sound. Vib.*, **315**(1-2), 318-342.

Iurlaro, L., Gherlone, M., Di Sciuva, M. and Tessler, A. (2013), "Assessment of the refined zigzag theory for bending, vibration, and buckling of sandwich plates: A comparative study of different theories", *Compos. Struct.*, **106**, 777-792.

Jung, W.Y., Han, S.C. and Park, W.T. (2014), "A modified couple stress theory for buckling analysis of S-FGM nanoplates embedded in Pasternak elastic medium", *Compos. Part B.*, **60**, 746-756.

Kiani, K. (2013), "Characterization of free vibration of elastically supported double-walled carbon nanotubes subjected to a longitudinally varying magnetic field", *Acta. Mech.*, **224**(12), 3139-3151.

Kiani, K. (2014a), "Free vibration of conducting nanoplates exposed to unidirectional in-plane magnetic fields using nonlocal shear deformable plates theories", *Physica. E.*, **57**, 179-192.

Kiani, K. (2014b), "Magnetically affected single-walled carbon nanotubes as nanosensors", *Mech. Res. Commun.*, **60**, 33-39.
Kiani, K. (2014c), "Revisiting the free transverse vibration of embedded single-layer graphene sheets acted upon by in-plane magnetic field", *J. Mech. Sci. Technol.*, **28**(9), 3511-3516.
Kiani, K. (2015a), "Elastic wave propagation in magnetically affected double-walled carbon nanotubes", *Meccanica*, **50**(4), 1003-2026.
Kiani, K. (2015b), "Column buckling of magnetically affected stocky nanowires carrying electric current", *J. Phys. Chem. Solids.*, **83**, 140-151.
Lei, Z.X., Liew, K.M. and Yu, J.L. (2012), "Buckling analysis of functionally graded carbon nanotube-reinforced composite plates using the element-free kp-Ritz method", *Compos. Struct.*, **98**, 160-168.
Li, Y.S. and Pan, E. (2015), "Static bending and free vibration of a functionally graded piezoelectric microplate based on modified couple stress theory", *Int. J. Eng. Sci.*, **97**, 40-59.
Lou, J., He, L., Du, J. and Wu, H. (2016), "Buckling and post-buckling analyses of piezoelectric hybrid microplate subject to thermo-electro-mechanical loads based on the modified couple stress theory", *Compos. Struct.*, **153**, 332-344.
Lou, J. and He, L. (2015), "Closed-form solutions for nonlinear bending and free vibration of FG microplates based on the modified couple stress theory", *Compos. Struct.*, **131**, 810-820.
Madani, H., Hosseini, H. and Shokravi, M. (2016), "Differential cubature for vibration analysis of embedded FG-CNT-reinforced piezoelectric cylindrical shells subjected to uniform and non-uniform temperature distributionbs", *Steel Compos. Struct., Int. J.*, **22**(4), 889-913.
Mizusawa, T. (1993), "Buckling of rectangular Mindlin plates with tapered thickness by the spline strip method", *Int. J. Solids. Struct.*, **30**(2), 1663-1677.
Mohammad Abadi, M. and Daneshmehr, A.R. (2014), "Size dependent buckling analysis of microbeams based on modified couple stress theory with high order theories and general boundry conditoins", *Int. J. Eng. Sci.*, **74**, 1-14.
Moita, J.S., Araújo, A.L., Franco Correia, V.M., Mota Soares, C.M. and Mota Soares, C.A. (2015), "Buckling and geometrically nonlinear analysis of sandwich structures", *Int. J. Mech. Sci.*, **92** 154-161.
Narendar, S., Gupta, S.S. and Gopalakrishnan, S. (2012), "Wave propagation in single-walled carbon nanotube under longitudinal magnetic field using nonlocal Euler-Bernolli beam theory", *Appl. Math. Model.*, **36**(9), 4529-4538.
Nateghi, A., Salamat-talab, M., Rezapour, J. and Daneshian, B. (2012), "Size dependent buckling analysis of functionally graded micro beams based on modified couple stress theory", *Appl. Math. Model.*, **36**(10), 4971-4987.
Rabani Bidgoli, M., Karimi, M. and Ghorbanpour Arani, A. (2015), "Viscous fluid induced vibration and instability of FG-CNT-reinforced cylindrical shells integrated with piezoelectric layers", *Steel Compos. Struct., Int. J.*, **19**(3), 713-733.
Ramamoorthy, M., Rajamohan, V. and AK, J. (2014), "Vibration analysis of a partially treated laminated composite magnetorheological fluid sandwich plate", *J. Vib. Control.*, **22**(3), 869-895.
Salvetat, D. and Rubio, A. (2002), "Mechanical properties of carbon nanotubes: a fiber digest for beginners", *Carbon*, **40**(10), 1729-1734.
Shen, H.S. (2009), "Nonlinear bending of functionally graded carbon nanotube-reinforced composite plates in thermal environments", *Compos. Struct.*, **91**(1), 9-19.
Shufrin, I. and Eisenberger, M. (2005), "Stability and vibration of shear deformable plates—first order and higher order analysis", *Int. J. Solids. Struct.*, **42**(3-4), 1225-1251.
Tessler, A., Di Sciuva, M. and Gherlone, M. (2009), "Refined Zigzag theory for laminated composite and sandwich plates", Technical, Report NASA-TP-2009-215561.
Tessler, A., Di Sciuva, M. and Gherlone, M. (2010), "A consistent refinement of first-order shear deformation theory for laminated composite and sandwich plates using improved zigzag kinematics", *J. Mech. Mater. Struct.*, **5**(2), 341-367.
Upadhyay, A.K. and Shukla, K.K. (2013), "Post-buckling behavior of composite and sandwich skew plates", *Int. Nonlinear Mech.*, **55**, 120-127.
Yas, M.H. and Samadi, N. (2012), "Free vibrations and buckling analysis of carbon nanotube-reinforced composite Timoshenko beams on elastic foundation", *Int. J. Pres. Ves. Pip.*, **98**, 119-128.
Zhang, D.G. and Zhou, H.M. (2015), "Mechanical and thermal post-buckling analysis of FGM rectangular plates with various supported boundaries resting on nonlinear elastic foundation", *Thin-Wall. Struct.*, **89**, 142-152.

CC

Appendix A

$$\begin{Bmatrix} K_1, K_2 \\ F_1, F_2 \\ B_1, B_2 \end{Bmatrix} = \int_{-h_1-\frac{h_m}{2}}^{-\frac{h_m}{2}} \left(\phi_1^a, \phi_2^a\right) \begin{Bmatrix} 1 \\ \frac{\partial}{\partial z} \\ z \end{Bmatrix} dz, \begin{Bmatrix} K_3, K_4 \\ F_3, F_4 \\ B_3, B_4 \end{Bmatrix} = \int_{-\frac{h_m}{2}}^{\frac{h_m}{2}} \left(\phi_1^b, \phi_2^b\right) \begin{Bmatrix} 1 \\ \frac{\partial}{\partial z} \\ z \end{Bmatrix} dz,$$

$$\begin{Bmatrix} K_5, K_6 \\ F_5, F_6 \\ B_5, B_6 \end{Bmatrix} = \int_{\frac{h_m}{2}}^{\frac{h_m}{2}+h_1} \left(\phi_1^c, \phi_2^c\right) \begin{Bmatrix} 1 \\ \frac{\partial}{\partial z} \\ z \end{Bmatrix} dz,$$

$$\begin{Bmatrix} E_{11}, E_{12}, E_{22} \\ F_{11}, F_{12}, F_{22} \end{Bmatrix} = \int_{-\frac{h_m}{2}-h_1}^{-\frac{h_m}{2}} \left(\phi_1^a\phi_1^a, \phi_1^a\phi_2^a, \phi_2^a\phi_2^a\right) \begin{Bmatrix} 1 \\ \frac{\partial}{\partial z} \end{Bmatrix} dz,$$

$$\begin{Bmatrix} E_{33}, E_{34}, E_{44} \\ F_{33}, F_{34}, F_{44} \end{Bmatrix} = \int_{-\frac{h_m}{2}}^{\frac{h_m}{2}} \left(\phi_1^b\phi_1^b, \phi_1^b\phi_2^b, \phi_2^b\phi_2^b\right) \begin{Bmatrix} 1 \\ \frac{\partial}{\partial z} \end{Bmatrix} dz,$$

$$\begin{Bmatrix} E_{55}, E_{56}, E_{66} \\ F_{55}, F_{56}, F_{66} \end{Bmatrix} = \int_{\frac{h_m}{2}}^{\frac{h_m}{2}+h_1} \left(\phi_1^c\phi_1^c, \phi_1^c\phi_2^c, \phi_2^c\phi_2^c\right) \begin{Bmatrix} 1 \\ \frac{\partial}{\partial z} \end{Bmatrix} dz,$$

$$\left\{R_{c1}^a, R_{c2}^a\right\} = \int_{-\frac{h_m}{2}-h_1}^{-\frac{h_m}{2}} \cos\left(\frac{\pi^2\left(-z-h_m/2\right)}{h_1^2}\right)\left\{\phi_1^a, \phi_2^a\right\} dz,$$

$$\left\{R_{c5}^c, R_{c6}^c\right\} = \int_{\frac{h_c}{2}}^{\frac{h_m}{2}+h_1} \cos\left(\frac{\pi^2\left(z-h_m/2\right)}{h_1^2}\right)\left\{\phi_1^c, \phi_2^c\right\} dz,$$

$$\begin{Bmatrix} P_{sa}^{\beta 1} \\ P_{sa}^{\beta 2} \end{Bmatrix} = \int_{-h_1-\frac{h_m}{2}}^{-\frac{h_m}{2}} -\sin\left(\frac{\pi\left(-z-1/2h_m\right)}{h_1}\right) \begin{Bmatrix} \frac{\partial}{\partial z}\phi_{1a} \\ \frac{\partial}{\partial z}\phi_{2a} \end{Bmatrix} dz,$$

$$\begin{Bmatrix} P_{sa}^{\beta 5} \\ P_{sa}^{\beta 6} \end{Bmatrix} = \int_{\frac{h_m}{2}}^{h_1+\frac{h_m}{2}} -\sin\left(\frac{\pi\left(z-1/2h_m\right)}{h_1}\right) \begin{Bmatrix} \frac{\partial}{\partial z}\phi_{1c} \\ \frac{\partial}{\partial z}\phi_{2c} \end{Bmatrix} dz,$$